

A refined position catalogue of the *Swift* XRT afterglows

A. Moretti¹, M. Perri², M. Capalbi², L. Angelini^{3,4}, J.E. Hill^{4,5}, S. Campana¹, D.N. Burrows⁶, J.P. Osborne⁷, G. Tagliaferri¹, G. Cusumano⁸, P. Giommi², P. Romano¹, T. Mineo⁸, J. Kennea⁶, D. Morris⁶, J. Nousek⁶, C. Pagani^{1,6}, J. Racusin⁶, A.F. Abbey⁷, A.P. Beardmore⁷, O. Godet⁷, M. R. Goad⁷, K.L. Page⁷, A.A. Wells⁷, G. Chincarini^{1,9}

¹ INAF, Osservatorio Astronomico di Brera, Via E. Bianchi 46, I-23807, Merate (LC), Italy

² ASI Science Data Center, via G. Galilei, I-00044 Frascati, Italy

³ NASA/Goddard Space Flight Center, Greenbelt Road, Greenbelt, MD20771, USA

⁴ Department of Physics and Astronomy, Johns Hopkins University, 3400 Charles Street, Baltimore, MD 21218, USA

⁵ Universities Space Research Association, 10211 Wincopin Circle, Suite 500, Columbia, MD, 21044-3432, USA

⁶ Department of Astronomy & Astrophysics, Pennsylvania State University, 525 Davey Lab, University Park, PA 16802, USA

⁷ X-Ray Observational Astronomy Group, Department of Physics & Astronomy, University of Leicester, LE1 7RH, UK

⁸ INAF, Istituto di Astrofisica Spaziale e Fisica Cosmica Sezione di Palermo, Via U. La Malfa 153, I-90146 Palermo, Italy

⁹ Università degli Studi di Milano-Bicocca, Dipartimento di Fisica, Piazza delle Scienze 3, I-20126 Milano, Italy

Received ; accepted

Abstract. We present a catalogue of refined positions of 68 gamma ray burst (GRB) afterglows observed by the *Swift* X-ray Telescope (XRT) from the launch up to 2005 Oct 16. This is a result of the refinement of the XRT boresight calibration. We tested this correction by means of a systematic study of a large sample of X-ray sources observed by XRT with well established optical counterparts. We found that we can reduce the systematic error radius of the measurements by a factor of two, from 6.5'' to 3.2'' (90% of confidence). We corrected all the positions of the afterglows observed by XRT in the first 11 months of the *Swift* mission. This is particularly important for the 37 X-ray afterglows without optical counterpart. Optical follow-up of dark GRBs, in fact, will be more efficient with the use of the more accurate XRT positions.

1. Introduction

The *Swift* satellite (Geherels et al 2004) detects and localises gamma ray bursts (GRBs) and provides autonomous rapid response observations and long term monitoring of their afterglow emission. The scientific payload consists of three instruments: the Burst Alert Telescope (BAT, Barthelmy et al. 2005), the X-ray Telescope (XRT, Burrows et al. 2005) and the UV/Optical Telescope (UVOT, Roming et al. 2005). *Swift* observations provide prompt γ -ray positions with an accuracy of few arcminutes, X-ray positions with an accuracy of few arcseconds and UV/Optical positions with accuracy of less than 1''. From the satellite launch (2004 Nov 20) to 2005 Oct 16, XRT observed 64 afterglows of GRBs detected by BAT and 5 afterglows of GRBs detected by other instruments (INTEGRAL and HETE-2).

For the same GRB sample only 31 optical counterparts were found either by UVOT or by ground-based telescopes. In most of the remaining cases stringent upper limits were set by deep optical observations. Classical explanations for burst optical darkness are, dust extinction, high redshift or intrinsic faintness. The study of the host galaxies through ultra-deep follow-up observations, is one of the most important ingredients for the determination of GRB progenitors. One of the key

factors in the follow-up is the accuracy of the GRB position. Before *Swift*, the study of the host galaxy was possible only in the presence of an optical afterglow detection (with the exception for the rare cases observed by XMM-Newton, *Chandra* or by radio telescopes), because of the limited position accuracy of the X-ray and γ -ray telescopes. This limitation could have produced some bias in the statistical study of the population of the host galaxies. For example, if we assume that the dust extinction plays an important role in the optical obscuration of the afterglow emission, the optically selected sample of host galaxies would have been biased against dust-rich galaxies. Now, by means of the *Swift* prompt automatic observations and the high quality of the XRT optics, we can obtain X-ray afterglow positions so accurate that the identification of the host galaxies is possible even when only the X-ray afterglow position is available. One of the goals of the XRT is to provide afterglow X-ray positions with the unprecedented accuracy of 5''. From a comparison of the XRT positions with the optical transients positions we find that, at present, 90% of the XRT positions are within a 6.5'' radius error circle, slightly worse than the pre-flight expectations. While the statistical uncertainties in the XRT position determination are well known, we find that the larger fraction of the error has a systematic origin. In the present work we show that we can correct for this systematic

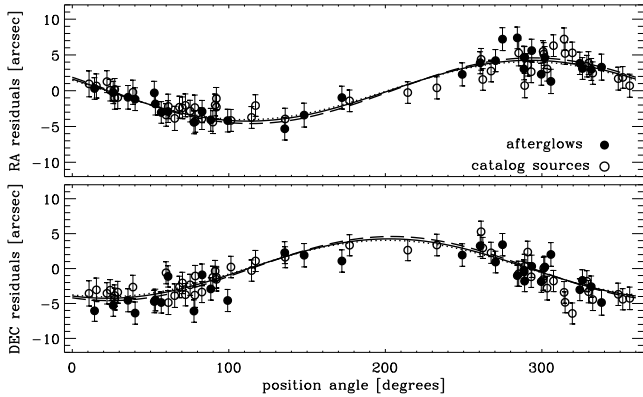


Fig. 1. Differences in coordinates (RA in the upper panel, DEC in the lower) between the XRT and optical positions (X-optical). We used both catalogued sources and GRB observations with well known optical counterpart. The plotted errors are the combination of the statistical errors and the aspect solution uncertainty. The solid line is the fit to the entire sample, the dashed line is the fit relative to the catalogued sources only and the dotted line is the fit to the afterglows: the best fit parameters are perfectly consistent. RA residuals have been corrected by the factor $\cos(\text{DEC})$, and represent the true separation in the sky.

error, improving the typical accuracy, and, using the proposed correction, we recalculated 68 X-ray afterglow positions.

2. The XRT position accuracy

For each GRB, XRT usually produces two position measurements: the on-flight rapid position and the refined on-ground position. The way the satellite works is that when the XRT observations starts promptly after the BAT trigger (100-200 s) and the X-ray flux is bright enough (~ 10 counts per second, corresponding to $\sim 5 \times 10^{-10}$ erg sec $^{-1}$ cm $^{-2}$), the first position measurement is calculated on-board by the flight software (Hill et al. 2004) and automatically distributed by the GRB Coordinate Network (GCN), typically within a few seconds of the spacecraft slewing and settling on the GRB. The XRT was able to calculate and distribute a rapid position, within 350 seconds from the burst trigger, in 19 cases. All the measured XRT positions are then refined on the ground using all the telemetered photon counting (PC) data from the first segment of the observation and sent again in a new GCN circular (see Hill et al. 2005 for a detailed description of the XRT automatic procedure). The uncertainties in the position measurements are determined by the statistical uncertainty and by the precision of the satellite pointing.

When the background rate is negligible, the statistical error in the position determination depends on the instrumental point spread function (PSF) and on the counts of the source according to the simple formula $U_{\text{stat}} \propto R_{90} / \sqrt{\text{counts}}$, where U_{stat} is 90% accuracy error circle radius and R_{90} is the radius which contains 90% of the fluence. The XRT statistical positional accuracy has been extensively tested on-ground and verified in flight during the calibration phase with some ad hoc obser-

vations (Hill et al. 2005; Moretti et al. 2005). We empirically found that the statistical error at the 90% level of XRT position measurement is given by the formula $U_{\text{stat}} = R \times \text{counts}^{-0.48}$ (Hill et al. 2004), with the parameter $R = 23''$, in very good agreement with the expectations. It means that for a source with more than 144 counts, the statistical error is less than $2''$. To determine the afterglow position, the flight software uses a very short exposure image (0.1 or 2.5 seconds): this means that the typical source counts to determine a centroid with are < 50 and therefore such positions are highly affected by statistical uncertainties. In telemetered PC mode data there are usually more than 150 counts and the statistical uncertainties in the on-ground refined position measurements are less than $2''$. We note that the expected background counts in a region containing 80% of the PSF in a typical exposure time of 20 ks, in the full energy band (0.2-10 keV), are ~ 2 and this fully justifies the previous assumption that the background is negligible.

In addition to the statistical error, the XRT position uncertainty is also determined by the uncertainty in the satellite aspect solution. The nominal value of this uncertainty is $3''$ as reported in the calibration file `swxposerr20010101v002.fits` (CALDB version 20050916).

In order to study the systematic errors, we collected all the XRT observations of point-like sources present in the public archive (<http://heasarc.gsfc.nasa.gov/cgi-bin/W3Browse/swift.pl>) from April to August 2005 with a catalogued optical position in the SIMBAD archive (<http://simbad.u-strasbg.fr/Simbad>), excluding the few with proper motion. Moreover, we added the 15 calibration observations of Mkn 876, RXJ0720.4-3125 and RXSJ1708-4009 taken between February 2005 and March 2005. We then considered all the observations of X-ray afterglows with a clearly varying optical counterpart published in the GCN in the period from December 2004 to September 2005. In order to select a very homogeneous sample and to minimize the statistical error, we selected the observations with the source at less than $3'$ from the center of the field of view and with more than 150 source counts. It resulted in a sample of 80 observations (31 afterglows and 49 catalogued sources). All the XRT data were reduced using the *xrtpipeline* task of the current release of the HEADAS software (version 1.6), with all the default options and the current release of the calibration files (CALDB version 20050916); then we calculated the XRT positions by means of the *xrtcentroid* task. As shown in Fig. 1, we found a clear relationship between the spacecraft position angle (PA, also called roll angle) of the observations and the residuals in RA and DEC of the X-ray positions in respect to the optical positions (note that RA residuals have been corrected by the factor $\cos(\text{DEC})$, and represent the true separation in the sky). The roll angle of an observation is the angle from sky coordinates to spacecraft coordinates and it is available in the header keyword `PA_PNT` of the event files.

We found that this relation is well fitted by a trigonometric function. A similar relation was already found for the MECS and LECS telescopes on board of the BeppoSAX satellite (Perri & Capalbi 2002). This effect is due to a small calibration error between the XRT boresight and the satellite star

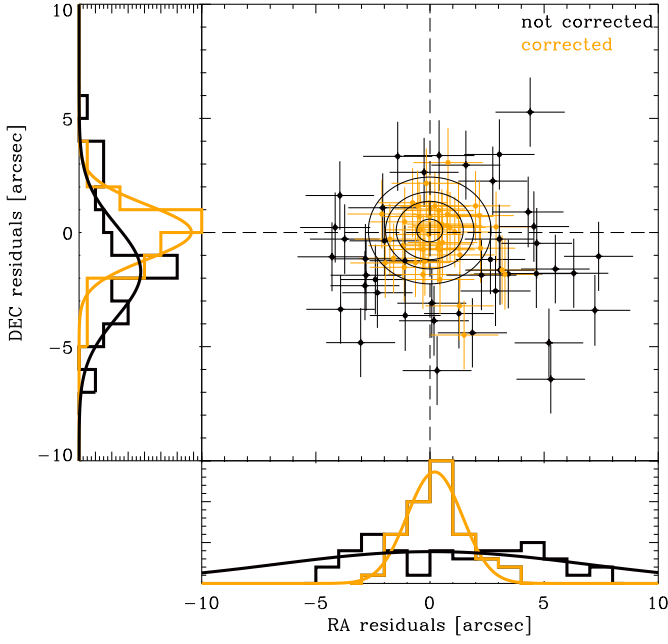


Fig. 2. The residuals of the 43 sources with more than 1000 counts before (black) and after the correction (grey). The contour of the two dimensional Gaussian best fit function are overplotted in correspondence of 10%, 50%, 90% of the maximum value. The external panels show the distribution of the coordinate residuals before and after the correction together with their best Gaussian fit.

tracker boresight, which causes a displacement of the detector system coordinate. The projection of this displacement in sky coordinates gives a dependence of the coordinates residuals with the roll angle. Therefore, we expect that we can fit together the two relations with the following functions

$$\Delta(\text{RA}) = M \sin(\text{PA} + \phi) \quad (1)$$

$$\Delta(\text{DEC}) = M \cos(\text{PA} + \phi) \quad (2)$$

where M is the amplitude of the misalignment and the phase ϕ is its direction. The best fit of the data is given by $M=4.2''\pm0.4''$ and $\phi = 157.6^\circ \pm 6.5^\circ$ (90% confidence errors), $\chi^2=0.8$ for 158 degrees of freedom. It corresponds to a shift of the nominal detector center of $1.8(\pm0.2)$ pixels (1 pixel is $2.36''$). A refinement of the boresight calibration will be included in the standard calibration files from Dec 2005 CALDB distribution. Because, as explained below, we will use this fit to correct all the afterglow positions, we checked whether the two subsamples (the catalogued sources and the afterglows) yield consistent results. As shown in Fig. 1, the fit of the two different sub-samples, as expected, give perfectly consistent results.

3. Correction of the systematic error

The parametrisation of the relationship between the coordinate residuals and the roll angle of the observations (Eqs. 1, 2) al-

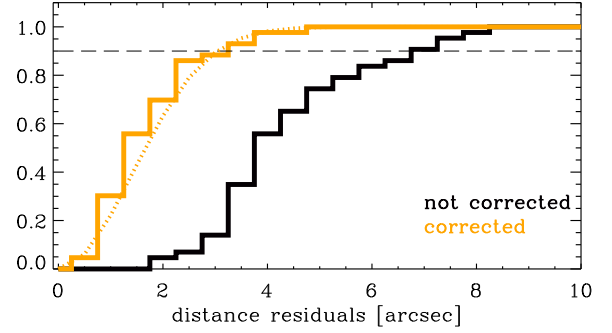


Fig. 3. The integral distribution of the distances of the X-ray sources, with more than 1000 counts, from the optical counterpart before (black lines) and after the correction (grey lines). The dotted line is the integral of the best Gaussian fit to the distribution of the coordinate residuals (see Fig. 2).

lows us to correct the source position derived from XRT observations with the following:

$$\text{RA}_{\text{new}} = \text{RA}_{\text{old}} - \Delta(\text{RA})/\cos(\text{DEC}) \quad (3)$$

$$\text{DEC}_{\text{new}} = \text{DEC}_{\text{old}} - \Delta(\text{DEC}). \quad (4)$$

First, we tested the goodness of the correction on the 43 sources in the sample with more than 1000 counts (statistical error $<1''$, Fig. 2). For all these 43 elements we calculated the distance between the optical position and the refined X-ray positions and we compared it with the uncorrected positions. Because for this particular source sub-sample the statistical uncertainty is negligible, this gives us the measurement of the systematic error.

In Fig. 3 we compare the distribution of the distances before and after the correction. From the integral distribution of the distances we find that 90% of the X-ray sources after the correction were within a distance of $3.2''$ (while the uncorrected value was $6.5''$). This is an improvement by a factor of ~ 4 in terms of error circle area. The mean of the distribution changes from $4.3''$ to $1.7''$ after the correction. We note that, as expected, the corrected residual distributions are well consistent with a Gaussian distribution. The Gaussian fit to the RA residual distribution yields -0.03 ± 0.18 , 1.2 ± 0.2 for the mean and standard deviation, respectively ($\chi^2 = 0.72$). The Gaussian fit to the DEC residual distribution yields 0.13 ± 0.20 , 1.3 ± 0.2 for the mean and standard deviation, respectively ($\chi^2 = 0.60$).

We then applied the boresight correction to the whole sample of 68 afterglows observed by XRT in PC mode from the launch to 2005 Oct 16. We retrieved all the first segments of the 68 PC observations from the *Swift* archive. We calculated the XRT positions by means of the *xrtcentroid* task. This task calculates the source centroids by recursively evaluating the barycentre in boxes reduced by 80% each time from the initial box size, which is an input parameter. If the statistical significance of the source is very low a too large detection box could affect the position determination. Possible sources of error are a background fluctuations or faint serendipitous sources present in the centroid box. In order to properly take into account for

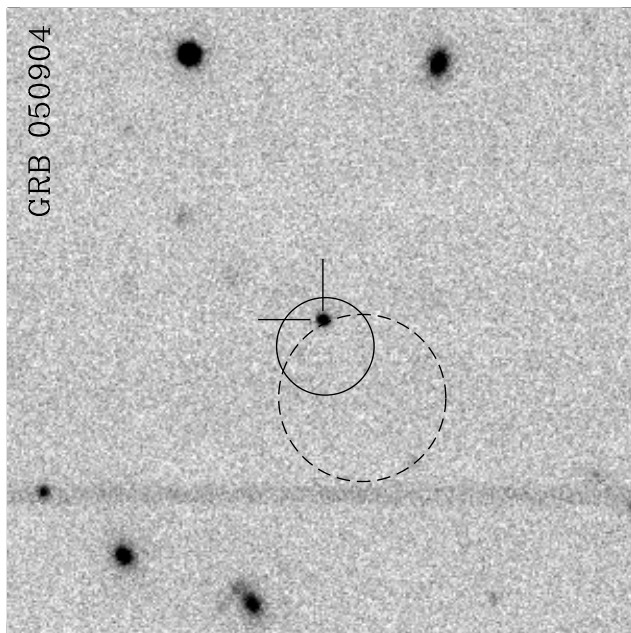


Fig. 4. A VLT+ISAAC J filter image of GRB 050904. The lines show the position of the optical afterglow. The dashed circle is the original error circle, while the smaller and solid line circle is the refined one. The optical transient is at $1.6''$ from the refined XRT position and at $6.2''$ from the original position quoted in Mineo et al. (2005). As it is clear from the distribution of the residuals (Fig. 3), this represents an extreme case: only 15% of the positions are expected to be at more than $6''$ from the optical position before the correction. The image is taken from Tagliaferri et al. (2005).

these effects we used the following procedure. First, we calculated the centroid with a fixed input error box size ($30''$); then we refined this position using different box sizes as function of the source counts, ranging from $30''$ (for bright sources) to $12''$ (for faint sources): for each source we used an initial box size such that the ratio between source and background counts, within the box, is always greater than 20, taking into account both the background rate and the PSF profile (Moretti et al. 2005). Finally we applied the boresight corrections (Eqs. 3,4) to the so calculated positions.

The refined positions are reported in Table 1; the quoted errors (90% confidence) are the quadratic sum of the statistical error with the new $3.2''$ systematic error. Moreover in the final error budget we added a term which depends on the source counts and which takes into account the uncertainty caused by the choice of the size of the xrtcentroid error box. We stress, however, that this term is negligible in most of the cases. The mean error of the sample is $3.7''$, and 90% of the afterglows have 90% confidence uncertainty less than $5''$. We stress that among the 68 new positions, 37 are of dark GRBs. We excluded GRB 050117 from our analysis because it does not have any useful PC mode data.

As an example of our results, in Fig. 4 we illustrate the case of GRB 050904 (Cummings et al. 2005), at redshift $z=6.3$

(Kawai et al. 2005). In this case the prompt observations from the ground allowed the detection of the IR transient (D’Avanzo et al. 2005). As shown in Fig. 4 the IR source position is right at the border of the original XRT error circle ($6''$ radius, Mineo et al. 2005), while it is perfectly contained by the refined one ($3.2''$). The measured colours of this afterglow do not show any hint of dust extinction (Tagliaferri et al. 2005). Had GRB 050904 been highly extinguished, it probably would have been undetectable by optical or IR observations. The search of the host galaxy would have been very hard because, although very close, the correct position at the border of the uncorrected XRT error circle.

4. Conclusion

We refined the boresight calibration of the XRT, resulting in a significant improvement of the position accuracy. The comparison with optical counterparts shows that on average we reduced the distance between XRT positions and optical positions by a factor of 2. This was possible by reducing the systematic error from $6.5''$ to $3.2''$ (90% confidence). By means of this correction we recalculated the position of 68 afterglows observed by XRT (the complete sample up to 2005 Oct 16). With one example, we showed how a deep follow-up study of the host galaxies of optically dark GRB can be performed with greater efficiency employing this correction. We note that after Oct 16 2005 the XRT afterglow positions provided by the XRT team in the GCNs are calculated with the new boresight calibration. Therefore, this work provides the complete catalogue of the refined XRT afterglow positions of the GRB preceding that date. For the subsequent observations of GRB afterglows, we stress that a refined boresight calibration will be implemented in the standard calibration products from the Dec 2005 CALDB distribution.

Acknowledgements. This work is supported at OAB-INAF by ASI grant I/R/039/04, at Penn State by NASA contract NAS5-00136 and at the University of Leicester by PPARC of grant PPA/Z/S/2003/00507. This research has made use of the SIMBAD database, operated at CDS, Strasbourg, France.

References

- Barthelmy, S.D., Barbier, L.M., Cummings, J.L., et al. 2005, *Sp.Sc.Rev.*, 120, 143
- Burrows, D.N., Hill, J.E., Nousek, J.A., et al. 2005, *Sp.Sc.Rev.*, 120, 165
- Cummings, J., Angelini L., Barthelmy S., et al. 2005, GCN 3910
- D’Avanzo, P., Antonelli, L.A., Covino S., et al. 2005 GCN 3921
- Gehrels, N., Chincarini, G., Giommi, P., et al. 2004, *ApJ*, 611, 1005
- Kawai, N., Yamada, T., Kosugi, G., Hattori, T., Aoki, K., 2005, GCN 3937
- Hill, J.E., Burrows, D.N., Nousek, J.A., et al. 2004, *proceedings of SPIE*, 5165, 217
- Hill, J.E., Angelini, L., Morris, D.C., et al. 2005, *proceedings of SPIE*, 5898, 313
- Mineo, T., Mangano, V., La Parola, V., et al. 2005, GCN 3920
- Moretti, A., Campana, S., Mineo, T., et al. 2005, *proceedings of SPIE*, 5898, 348
- Perri, M., Capalbi M., 2002, *A&A* 396, 753

Table 1. Refined positions and 90% statistical and systematic position error radii for the whole sample of 68 GRB afterglows observed by the Swift XRT.

GRB	RA(J2000)	DEC(J2000)	unc.(90%)["]	GRB	RA(J2000)	DEC(J2000)	unc.(90%)["]
041223	06 40 47.43	-37 04 25.2	3.4	050713B	20 31 15.51	+60 56 44.6	3.3
050124	12 51 30.33	+13 02 42.8	3.5	050714	02 54 22.93	+69 06 46.3	5.1
050126	18 32 27.13	+42 22 14.7	3.5	050714B	11 18 47.66	-15 32 48.9	3.3
050128	14 38 17.78	-34 45 52.6	3.2	050716	22 34 20.77	+38 41 03.0	3.3
050215B	11 37 47.70	+40 47 47.1	4.5	050717	14 17 24.60	-50 32 00.0	3.3
050219	11 05 39.03	-40 41 00.8	4.1	050721	16 53 44.62	-28 22 52.1	3.3
050219B	05 25 15.87	-57 45 29.9	3.4	050724	16 24 44.64	-27 32 25.3	3.4
050223	18 05 33.08	-62 28 20.5	5.4	050726	13 20 11.95	-32 03 50.6	3.3
050306	18 49 14.48	-09 09 10.0	4.9	050730	14 08 17.22	-03 46 18.8	3.2
050315	20 25 54.13	-42 35 59.8	3.2	050801	13 36 35.37	-21 55 42.1	3.4
050318	03 18 50.77	-46 23 44.8	3.3	050802	14 37 05.84	+27 47 10.8	3.2
050319	10 16 47.80	+43 32 54.9	3.2	050803	23 22 37.90	+05 47 08.8	3.2
050326	00 27 49.18	-71 22 14.6	3.6	050813	16 07 57.07	+11 14 54.2	6.5
050401	16 31 28.85	+02 11 14.4	3.3	050814	17 36 45.43	+46 20 22.3	3.3
050406	02 17 52.39	-50 11 14.9	3.8	050815	19 34 22.94	+09 08 50.8	3.5
050408	12 02 17.35	+10 51 09.6	3.3	050819	23 55 01.45	+24 51 35.3	3.7
050410	05 59 12.74	+79 36 09.8	4.0	050820	22 29 38.16	+19 33 35.1	3.2
050412	12 04 25.19	-01 12 00.4	4.2	050820B	09 02 25.48	-72 38 43.3	4.1
050416	12 33 54.63	+21 03 27.3	3.3	050822	03 24 27.09	-46 01 59.6	3.3
050421	20 29 03.18	+73 39 18.2	3.5	050824	00 48 56.23	+22 36 31.2	3.4
050422	21 37 54.92	+55 46 45.3	3.7	050826	05 51 01.49	-02 38 38.6	3.4
050502B	09 30 10.01	+16 59 47.1	3.3	050827	04 17 09.58	+18 12 00.2	3.4
050504	13 24 01.19	+40 42 15.7	5.3	050904	00 54 50.82	+14 05 08.2	3.2
050505	09 27 03.19	+30 16 22.7	3.2	050908	01 21 50.65	-12 57 19.0	3.4
050509	20 42 19.86	+54 04 16.3	4.6	050915	05 26 44.81	-28 01 00.3	3.4
050509B	12 36 13.56	+28 59 01.7	7.6	050915B	14 36 26.26	-67 24 32.1	3.4
050520	12 50 05.77	+30 27 03.7	4.7	050916	09 03 56.98	-51 25 46.6	3.3
050522	13 20 34.63	+24 47 20.4	9.2	050922B	00 23 13.23	-05 36 17.2	3.2
050525	18 32 32.63	+26 20 21.5	3.4	050922C	21 09 33.12	-08 45 29.6	3.3
050603	02 39 56.82	-25 10 55.2	3.5	051001	23 23 48.77	-31 31 20.9	3.5
050607	20 00 42.78	+09 08 30.5	3.3	051006	07 23 14.02	+09 30 19.5	3.4
050701	15 09 01.67	-59 24 53.7	3.7	051008	13 31 29.50	+42 05 55.7	3.2
050712	05 10 48.00	+64 54 48.0	3.3	051016	08 11 16.65	-18 17 55.1	3.5
050713	21 22 09.78	+77 04 28.9	3.3	051016B	08 48 27.70	+13 39 18.8	3.3

Roming, P.W.A., Kennedy, T.E., Mason, K.O., et al. 2005, Sp.Sc.Rev.,
120, 95

Tagliaferri, G., Antonelli, L.A., Chincarini, G., et al. 2005, A&A 443,
L1